Src-mediated caveolin-1 phosphorylation affects the targeting of active Src to specific membrane sites

Efrat Gottlieb-Abraham[a], Dmitry E. Shvartsman[a,*], John C. Donaldson[b,†], Marcelo Ehrlich[c], Orit Gutman[a], G. Steven Martin[b], and Yoav I. Henis[a]

[a]Department of Neurobiology and [c]Department of Cell Research and Immunology, George S. Wise Faculty of Life Sciences, Tel Aviv University, Tel Aviv 69978, Israel; [b]Department of Molecular and Cell Biology, University of California, Berkeley, Berkeley, CA 94720

ABSTRACT **Src interactions with the plasma membrane are an important determinant of its activity. In turn, Src activity modulates its association with the membrane through binding of activated Src to phosphotyrosylated proteins. Caveolin-1 (Cav-1), a major component of caveolae, is a known Src phosphorylation target, and both were reported to regulate cell transformation. However, the nature of Src-Cav-1 interactions, a potential mechanism of their coregulation, remained unclear. Here we used fluorescence recovery after photobleaching beam-size analysis, coimmunoprecipitation, quantitative imaging, and far-Western studies with cells expressing wild type, as well as structural and activity mutants of Src–green fluorescent protein and Cav-1–monomeric red fluorescent protein, to measure their interactions with the membrane and with each other. We show dynamic Src–plasma membrane interactions, which are augmented and stabilized by Cav-1. The mechanism involves phosphorylation of Cav-1 at Tyr-14 by Src and subsequent binding of the Src SH2 domain to phospho–Cav-1, leading to accumulation of activated Src in focal adhesions. This novel Cav-1 function potentially modulates focal adhesion dynamics.**

Monitoring Editor
Keith E. Mostov
University of California, San Francisco

Received: Mar 27, 2013
Revised: Oct 7, 2013
Accepted: Oct 8, 2013

INTRODUCTION

The nonreceptor protein-tyrosine kinase c-Src is the prototype of the Src family of protein kinases (SFKs). It is associated with the plasma membrane, endosomal compartments, and cell adhesions and mediates responses involved in cellular differentiation, adhesion, and migration (Kaplan *et al.*, 1992; Brown and Cooper, 1996; Schlaepfer *et al.*, 1999; Abram and Courtneidge, 2000; Sandilands *et al.*, 2007). Constitutively active Src can transform cells in vitro (Martin, 2001; Courtneidge, 2002; Frame, 2004), and increased c-Src expression or activity has been detected in multiple types of human cancer (Bjorge *et al.*, 2000; Frame, 2002; Ishizawar and Parsons, 2004). The first 16 N-terminal residues of Src (residue numbers refer to chicken c-Src) contain an N-myristoylation site and a series of basic residues, both required for membrane association (Resh, 1999, 2006). This association is critical for Src signaling and intracellular distribution (Kamps *et al.*, 1985; Buss *et al.*, 1986; Resh, 1999, 2006). The N-terminal membrane anchor is followed by two protein interaction modules, the SH3 and SH2 domains, which are required both for inactivating intramolecular interactions and for Src targeting to and phosphorylation of protein substrates (Martin, 2001; Frame, 2004; Shvartsman *et al.*, 2007; Oneyama *et al.*, 2008). The other half of the molecule contains the Src kinase domain, which mediates most of its biological functions, and a C-terminal regulatory domain; phosphorylation of Tyr-527 in this domain by C-terminal Src kinase (Csk) confers an inactive closed conformation, whereas mutations that prevent this phosphorylation (such as Y527F) result in a constitutively active open conformation (Martin, 2001;

This article was published online ahead of print in MBoC in Press (http://www.molbiolcell.org/cgi/doi/10.1091/mbc.E13-03-0163) on October 16, 2013.

Present addresses: *School of Engineering and Applied Sciences and Wyss Institute, Harvard University, Cambridge, MA 02138; †Thermo Fisher Scientific, Fremont, CA 94538.

Address correspondence to: Yoav I. Henis (henis@post.tau.ac.il).

Abbreviations used: Cav-1, caveolin-1; Cbp, Csk-binding protein; Csk, C-terminal Src kinase; FA, focal adhesion; FRAP, fluorescence recovery after photobleaching; GST, glutathione *S*-transferase; pCav-1, pY14-Cav-1; PDGF, platelet-derived growth factor; SFK, Src family of protein kinases; WT, wild type.

Courtneidge, 2002; Frame, 2004). Using fluorescence recovery after photobleaching (FRAP) and FRAP beam-size analysis, we show that tyrosine phosphorylation of membrane proteins by Src is followed by binding of activated Src to the phosphorylated tyrosine (pTyr) sites via its SH2 domain and that this binding regulates Src membrane interactions and localization (Shvartsman *et al.*, 2007).

The membrane association and intracellular distribution of SFKs depend on their unique fatty-acylated N-terminal sequences (Brown and Cooper, 1996; Resh, 1999, 2006; Sandilands *et al.*, 2007). Apart from the common N-myristoylation site, most SFKs (e.g., Fyn and Yes) contain one or two N-terminal palmitoylation sites, which are absent in Src (Resh, 1999). Palmitoylation is important for targeting membrane-associated proteins to cholesterol-enriched, dynamic membrane assemblies commonly referred to as lipid rafts (Simons and Toomre, 2000; Hancock, 2006; Jacobson *et al.*, 2007) and/or to caveolin-based caveolae, which can be viewed as a subset of rafts (Simons and Toomre, 2000; Anderson and Jacobson, 2002; Parton *et al.*, 2006). Palmitoylated SFKs are targeted to rafts/caveolae (Shenoy-Scaria *et al.*, 1994; Robbins *et al.*, 1995; Resh, 1999; Oneyama *et al.*, 2009), whereas the single myristoyl in Src is insufficient for raft association (Melkonian *et al.*, 1999; Oneyama *et al.*, 2009). Accordingly, Src localization was reported to be mainly non-raft (Shenoy-Scaria *et al.*, 1994; Mukherjee *et al.*, 2003; Oneyama *et al.*, 2008), although some reports suggest partial association with rafts (Tansey *et al.*, 2000; Veracini *et al.*, 2006). This conflict may reflect the major role of tyrosine-phosphorylated membrane proteins such as Csk-binding protein (Cbp, also called PAG) in recruiting Src to rafts/caveolae (Oneyama *et al.*, 2008, 2009).

Caveolin-1 (Cav-1) is the major protein component of caveolae (Liu *et al.*, 2002; Razani *et al.*, 2002; Parton *et al.*, 2006). It was first identified as a tyrosine phosphorylation target of v-Src in Rous sarcoma virus–transformed cells (Glenney and Zokas, 1989; Glenney and Soppet, 1992) and was found to be phosphorylated by Src at Tyr-14 (Li *et al.*, 1996b; Aoki *et al.*, 1999; Lee *et al.*, 2000) to produce pY14–Cav-1 (pCav-1). This phosphorylation has multiple functions, from recruitment of SH2-containing proteins (e.g., Csk or Grb7; Lee *et al.*, 2000; Cao *et al.*, 2002) to regulation of various cellular processes (Parat *et al.*, 2003; del Pozo *et al.*, 2005; Gaus *et al.*, 2006; Grande-Garcia *et al.*, 2007; Urra *et al.*, 2012). pCav-1 was reported to be present at or near focal adhesions (FAs; Lee *et al.*, 2000; del Pozo *et al.*, 2005; Gaus *et al.*, 2006) and to enhance FA dynamics (Joshi *et al.*, 2008). However, this view was challenged by a study showing that the monoclonal anti–pY14-Cav-1 antibody used in the earlier studies also labels paxillin (Hill *et al.*, 2007).

The nature of the Src–Cav-1 interaction is unclear. Initially, it was proposed that it depends on the Cav-1 scaffolding domain and shows high preference for wild-type Src (Src-WT) over activated (viral) Src (Li *et al.*, 1996a). In contrast, a later study suggested that Cav-1 phosphorylation by Src depends on Cav-1 palmitoylation at Cys156 (Lee *et al.*, 2001). However, more recent studies showed that Src is recruited to rafts/caveolae mainly by binding of its SH2 domain to phosphorylated Cbp, suggesting recruitment of activated Src; of note, the confinement to rafts/caveolae by raft-anchored Cbp suppressed SFK-mediated cell transformation (Oneyama *et al.*, 2008, 2009; Resh, 2008). This raises the intriguing possibility that Cav-1, which resembles Cbp in being a raft-localized Src phosphorylation target and in its ability to recruit Csk (Glenney and Zokas, 1989; Li *et al.*, 1996b; Cao *et al.*, 2002; Place *et al.*, 2011), can regulate Src signaling by targeting active Src to specific membrane regions. Here we show that after phosphorylation of Cav-1 by Src at Tyr-14, activated Src binds directly to pCav-1 via its SH2 domain. This interaction, which is sensitive to cholesterol depletion, selectively enhances the association of active Src with the plasma membrane, retards its lateral diffusion, and preferentially targets active Src to FAs, opposite to the effect of Cbp.

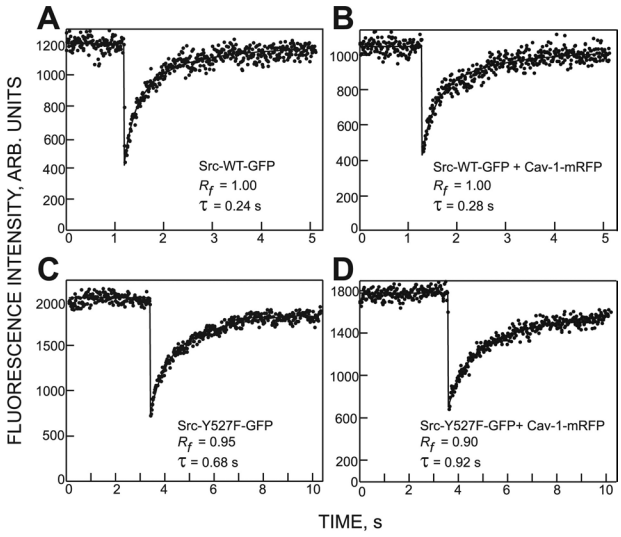

FIGURE 1: Typical curves showing that Cav-1 expression preferentially reduces the FRAP rate of constitutively active Src-Y527F-GFP. FRAP experiments were conducted at 22°C using the 63× objective, as described under *Materials and Methods*, on COS-7 cells transiently transfected with Src-WT-GFP (A), Src-WT–GFP + Cav-1–mRFP (B), Src-Y527F-GFP (C), or Src-Y527F-GFP + Cav-1 (D). Solid lines show the best fit of a nonlinear regression analysis, with the resulting τ and R_f values.

RESULTS

Cav-1 selectively enhances membrane association of activated Src

To investigate the effects of Cav-1 on the dynamics of Src interactions with the plasma membrane and their potential dependence on its activation state, we expressed Src-WT–green fluorescent protein (GFP) or constitutively active Src-Y527F-GFP alone or together with Cav-1–monomeric red fluorescent protein (mRFP) in COS-7 cells, which were then subjected to FRAP-beam size analysis. Typical results are shown in Figure 1, and quantitative data summarizing experiments on multiple cells are depicted in Figure 2. The analysis used two laser beam sizes, generated using a 63× (smaller Gaussian radius, ω) or a 40× (larger ω) objective (Henis *et al.*, 2006). The ratio between the illuminated areas, $\omega^2(40\times)/\omega^2(63\times)$, was 2.28. For FRAP by lateral diffusion, τ ($t_{1/2}$ for recovery) reflects the characteristic diffusion time τ_D, which is proportional to the laser-bleached area ($\tau_D = \omega^2/4D$, where D is the lateral diffusion coefficient). Therefore, for FRAP by lateral diffusion, the $\tau(40\times)/\tau(63\times)$ ratio should equal the beam-size ratio (2.28). On the other hand, a τ ratio of 1 is indicative of FRAP by exchange between membrane-associated and cytoplasmic pools of the protein. In this case, τ is the characteristic exchange time τ_{ex}, which is independent of the beam size. Intermediate τ ratios suggest mixed recovery (Henis *et al.*, 2006; Shvartsman *et al.*, 2007).

As shown in Figures 1 and 2, the recovery rate of Src-Y527F-GFP was significantly slower than that of Src-WT-GFP, accompanied by a much higher $\tau(40\times)/\tau(63\times)$ ratio for the constitutively active mutant. In fact, the τ ratio of Src-Y527F-GFP was not significantly different from the 2.28 beam-size ratio expected for recovery by pure lateral

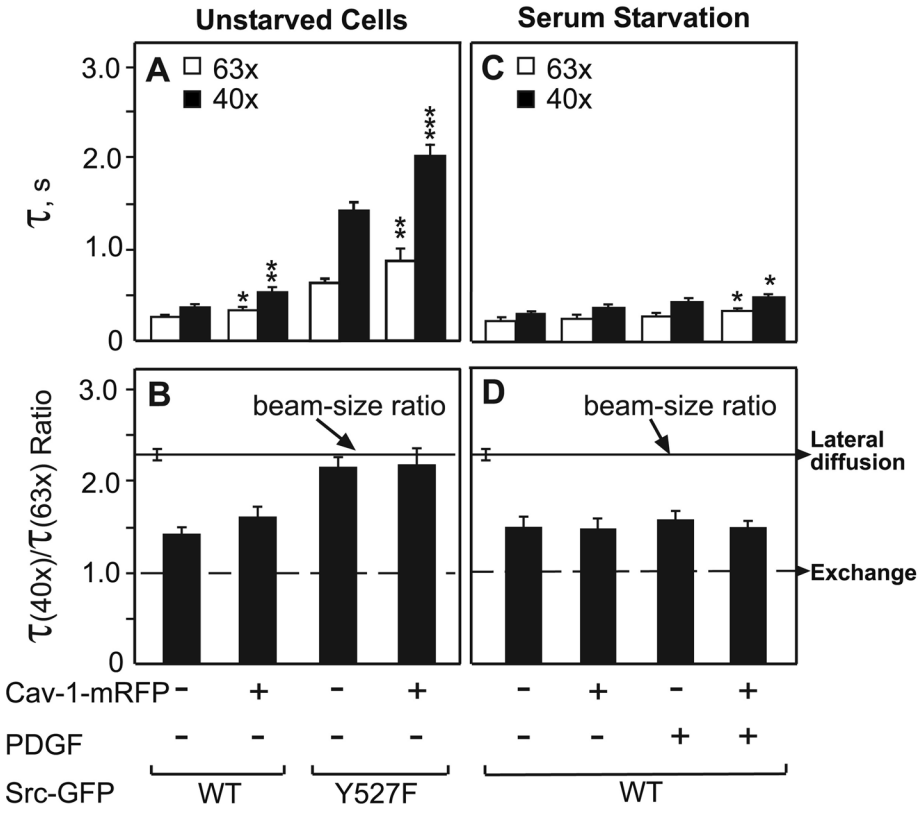

FIGURE 2: FRAP beam-size analysis of the effects of Cav-1 expression on the membrane interactions of Src-WT-GFP and Src-Y527F-GFP. COS-7 cells were cotransfected with a vector encoding a Src-GFP derivative together with a Cav-1–mRFP–encoding vector or empty vector (see *Materials and Methods*). After 24 h, FRAP beam-size analysis was conducted at 22°C on cells grown in 10% FCS (A , B) or on serum-starved cells with or without PDGF stimulation (C, D). FRAP experiments were conducted on Src-GFP (see *Materials and Methods*), identifying Cav-1–mRFP–expressing cells by mRFP fluorescence. Bars are means ± SEM of 30–60 measurements. The studies used 40× and 63× objectives, yielding a 2.28 ± 0.17 ($n = 59$) beam-size ratio. Thus this ratio (solid lines in B or D) is expected for FRAP by lateral diffusion. A τ ratio of 1 (dashed lines) is expected for recovery by exchange (Henis *et al.*, 2006). The R_f values were high in all cases (0.92–0.96). (A, C) τ values. Asterisks indicate significant differences from τ(63×) or τ(40×), comparing the same Src-GFP protein ± Cav-1–mRFP (*$p < 0.05$; **$p < 2 \times 10^{-5}$; ***$p < 10^{-7}$; Student's *t* test). The dependence of the Cav-1 effect on Src activity is demonstrated by the weaker effect of Cav-1 on Src-WT. Moreover, the effect of Cav-1 on Src-WT appears to be due to serum activation of Src-WT, as it disappears after serum starvation (C, D). PDGF stimulation restored some of the Cav-1–mediated retardation; the effect is only partial, consistent with the notion that PDGF activates only a fraction of the Src-WT population (C). (B, D) τ(40×)/τ(63×) ratios. Bootstrap analysis (see *Materials and Methods*) shows that only the τ ratio of Src-WT (with or without Cav-1) is significantly different from the 2.28 beam-size ratio ($p < 10^{-5}$). This suggests that Src-WT has a lower affinity to the PM, resulting in mixed-mode FRAP (lateral diffusion and exchange).

diffusion. This enables us to calculate *D* directly from the τ value (which is τ_D in this case), yielding 0.22 μm²/s. On the other hand, the τ ratio of Src-WT-GFP was intermediate between 2.28 and 1 (the ratio expected for recovery by exchange), suggesting weaker membrane interactions for Src-WT-GFP, which lead to faster dissociation from the membrane. The contribution of exchange does not permit accurate calculation of *D*, which, however, can be estimated from the τ(63×) value, as the smaller bleach area reduces τ_D, resulting in a higher contribution to the FRAP of lateral diffusion relative to exchange (Shvartsman *et al.*, 2007). This calculation yields $D = 0.64$ μm²/s for Src-WT-GFP. These findings are in good agreement with our earlier results on Src-WT and Src-Y527F (Shvartsman *et al.*, 2007). Of importance, coexpression with Cav-1–mRFP resulted in a small, albeit significant increase in the τ values of Src-WT-GFP and a marked increase in the τ values of Src-Y527F-GFP (Figures 1 and 2A). Thus coexpression with Cav-1–mRFP decreased the *D* values of Src-Y527F-GFP from 0.22 to 0.16 μm²/s. Both values are significantly slower than the *D* values obtained on the same cells for a lipid probe (1 μm²/s; Rotblat *et al.*, 2004) or for Src-WT-GFP (0.64 μm²/s), suggesting that the lateral diffusion of activated Src is retarded by interaction with slower-diffusing membrane proteins, including Cav-1 itself. These interactions must be transient, since they reduce the τ value of Src-Y527F rather than its mobile fraction. The limited effect of Cav-1 on the FRAP rates of Src-WT-GFP appears to be due to activation of a small fraction of Src-WT in the presence of serum, since under serum-starvation conditions the effects of Cav-1 on Src-WT-GFP recovery rates disappeared, whereas stimulation by platelet-derived growth factor (PDGF) restored the retardation of Src-WT-GFP diffusion by Cav-1 (Figure 2C). Note that reducing the expression of endogenous Cav-1 by Cav-1 small interfering RNA (siRNA) did not have a significant effect on Src-Y527F-GFP recovery in the FRAP studies (Figure 3), in line with our earlier demonstration that the lateral diffusion of Src-Y527F is retarded by interactions with multiple pTyr membrane protein targets (Shvartsman *et al.*, 2007). Because Src-Y527F-GFP is overexpressed relative to endogenous Cav-1, only a small fraction of Src-Y527F can bind to endogenous Cav-1, rendering the Cav-1 effect on Src-Y527F-GFP mobility undetectable. On overexpression of Cav-1, the fraction of membrane-associated Src-Y527F bound to Cav-1 increases, enabling the detection of the additional retardation by FRAP. Thus it is not feasible to fully prove functional Src-pCav-1 interactions at endogenous levels, and such confirmation should await further studies.

To complement these studies and corroborate the biophysical results with biochemical data, we measured Src–Cav-1 interactions by coimmunoprecipitation studies on cells expressing Src-WT-GFP or Src-Y527F-GFP with or without Cav-1–mRFP (Figure 4). Src-GFP proteins were precipitated from cell lysates with anti-Src or anti-GFP antibodies, followed by immunoblotting with antibodies to Cav-1, pCav-1, or GFP. Two bands of Cav-1–mRFP, one above and one just below 50 kDa, are coprecipitated with Src (Figure 4A). The upper band represents pCav-1 (Figure 4C), as demonstrated by its absence in 1) lysates of cells coexpressing Cav-1–mRFP and catalytically inactive Src-Y527F/K295M (see Figure 6C, Cav-1 blot, lane 4) and 2) lysates of cells coexpressing Src-Y527F and Cav-1–Y14F (see Figure 7C, panel 3, lane 3). Whereas pCav-1 represents a minor fraction of the total Cav-1 pool detected in cell lysates (Figure 4A, panel 3), it is highly enriched in the Src immunoprecipitates (top), suggesting a highly

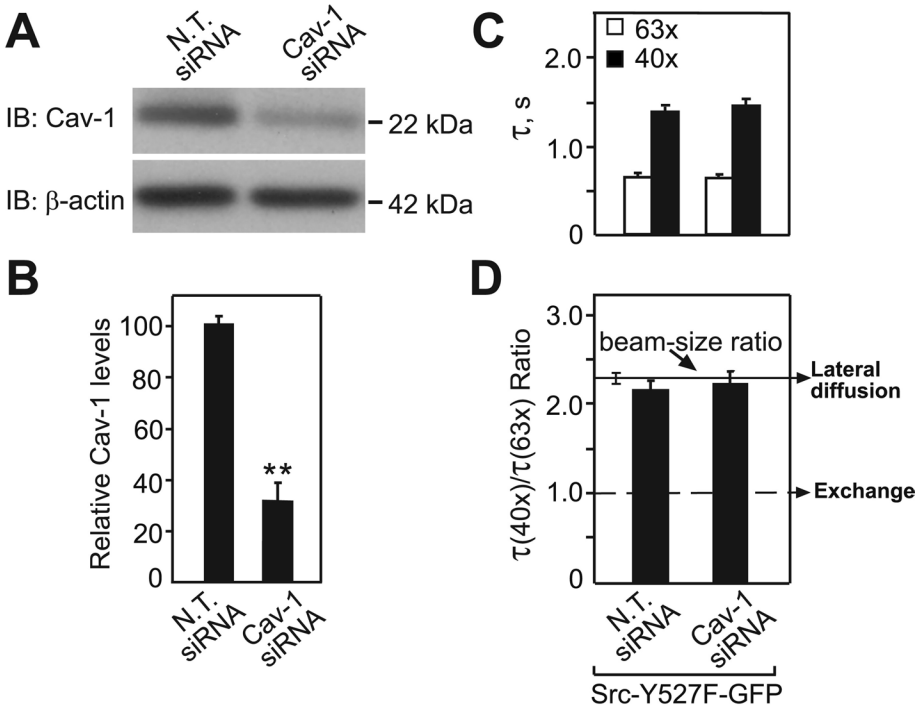

FIGURE 3: siRNA-mediated depletion of Cav-1 does not affect significantly the FRAP kinetics of Src-Y527F-GFP. COS-7 cells grown in six-well plates were cotransfected with Src-Y527F-GFP together with 50 nM human Cav-1 siRNA or nontargeting (N.T.) siRNA (see *Materials and Methods*). After 48 h, cells were lysed and immunoblotted (IB) with anti–Cav-1 or anti–β-actin (A, B) or subjected to FRAP beam-size analysis as in Figure 2 (C, D). (A, B) Western blot analysis shows effective knockdown of endogenous Cav-1. A typical experiment is shown in A, and quantification ($n = 3$) is depicted in B. Quantification after normalization to the loading control (β-actin) yielded reduction ± SEM by ~70%. Asterisks indicate a significant reduction in the Cav-1 level after treatment with Cav-1 siRNA (**$p < 0.01$, Student's t test). (C) τ values. Bars, means ± SEM of 30–60 FRAP measurements. Comparison of the effects of coexpression of Cav-1 siRNA with those of nontargeting siRNA on the τ(63×) or τ(40×) values of Src-Y527F-GFP shows no significant differences. (D) τ(40×)/τ(63×) ratios. No significant differences were observed.

preferential association of pCav-1 with Src. Quantification of several such experiments (Figure 4B) shows that Src-Y527F coprecipitates a significantly higher amount of pCav-1 than Src-WT. These conclusions are further validated by the coprecipitation of pCav-1 (detected using anti–pCav-1 antibodies) with Src-Y527F-GFP and Src-WT-GFP (Figure 4, C and D). Moreover, the same phenomenon was observed for the coprecipitation of endogenous pCav-1 with the Src-GFP proteins (Figure 4, E and F). The increased interaction of Src-Y527F with pCav-1 detected in the immunoprecipitation assays correlates with the biophysical studies, indicating a high level of interaction of Cav-1 with active Src in live cells (Figures 1 and 2).

Interactions of activated Src with Cav-1 are cholesterol dependent

In view of the association of Cav-1 with cholesterol-enriched assemblies, particularly caveolae, we examined the effects of cholesterol depletion on the ability of Cav-1–mRFP overexpression to retard the lateral diffusion of Src-Y527F-GFP. To this end, cholesterol was depleted (or not; control) using metabolic inhibition of its synthesis (see *Materials and Methods*), and cells expressing Src-Y527F-GFP (with or without Cav-1) were subjected to FRAP beam-size analysis (Figure 5, A and B). Cholesterol depletion eliminated the Cav-1–mediated retardation in the lateral diffusion rate of Src-Y527F-GFP (Figure 5A), retaining the τ ratio at a level close to that of recovery by lateral diffusion (Figure 5B). The observed effects of cholesterol depletion were on the interactions between activated Src and Cav-1 rather than on the levels of pCav-1 or Cav-1, which remained unchanged (Figure 5, C and D), whereas the level of pCav-1 coprecipitated with Src-Y527F was reduced significantly (Figure 5, C and E). These findings are consistent with the notion that the Cav-1–mediated retardation of Src-Y527F-GFP mobility is cholesterol dependent.

Cav-1–Src interactions require the Src SH2 domain and the phosphorylation of Cav-1 Tyr-14 by Src

To examine the roles of the different Src domains in its interactions with Cav-1, we coexpressed Cav-1–mRFP with Src-Y527F-GFP or the same protein carrying a second mutation that disabled a specific domain/function (kinase-dead Src-Y527F/K295M, SH2-defective Src-Y527F/R175A, or SH3-defective Src-Y527F/W118A). The cells were subjected to FRAP beam-size analysis to measure the effects of Cav-1 on Src-GFP membrane interaction dynamics. In accord with our previous studies (Shvartsman *et al.*, 2007), loss of Src kinase activity or SH2 function led to faster lateral diffusion, reflecting reduced binding to pTyr-protein targets in the plasma membrane (Figure 6A). On the other hand, the SH3-defective mutant not only did not diffuse faster, but even exhibited slower lateral diffusion, most likely due to its enhanced kinase activity, which generates more pTyr-protein targets at the plasma membrane (Erpel *et al.*, 1995; Shvartsman *et al.*, 2007). Concomitantly, the τ ratio of this mutant was decreased, suggesting a somewhat increased contribution of exchange, as discussed by us earlier (Shvartsman *et al.*, 2007). Figure 6A shows that the retardation of the lateral diffusion of Src-Y527F mutants by Cav-1 also requires both the Src kinase activity and the function of its SH2 domain; the resemblance to the findings with the general population of pTyr-protein targets holds also for the SH3 mutant (Figure 6A), which exhibits somewhat stronger binding of pCav-1 than Src-Y527F (Figure 6D). Note that the lateral diffusion of the SH3 mutant is not further retarded by Cav-1 coexpression, most likely because this mutant is already maximally associated with a multitude of pTyr-protein targets in the membrane (Figure 6A). Although Cav-1 induces a minor increase in the Src-Y527F/W118A τ ratio (Figure 6B), it is below the significance limit. These conclusions were validated by coimmunoprecipitation studies of lysates of similarly transfected cells (Figure 6, C and D), which showed that pCav-1 coprecipitated with Src-Y527F and with the SH3-defective mutant Src-Y527F-W118A (validating that they still interact) but not with the catalytically inactive Src-Y527F/K295M or the SH2-defective Src-Y527F/R175A.

To investigate the role of specific motifs in Cav-1 on its ability to modulate Src membrane interactions, we used FRAP beam-size analysis to investigate the effects of coexpression of a series of Cav-1–mRFP mutants on the mobility of Src-Y527F-GFP (Figure 7, A and B). Mutation of the Cav-1 Tyr14 to Phe, which eliminates the Tyr14 phosphorylation site, abolished the retarding effect of Cav-1 on

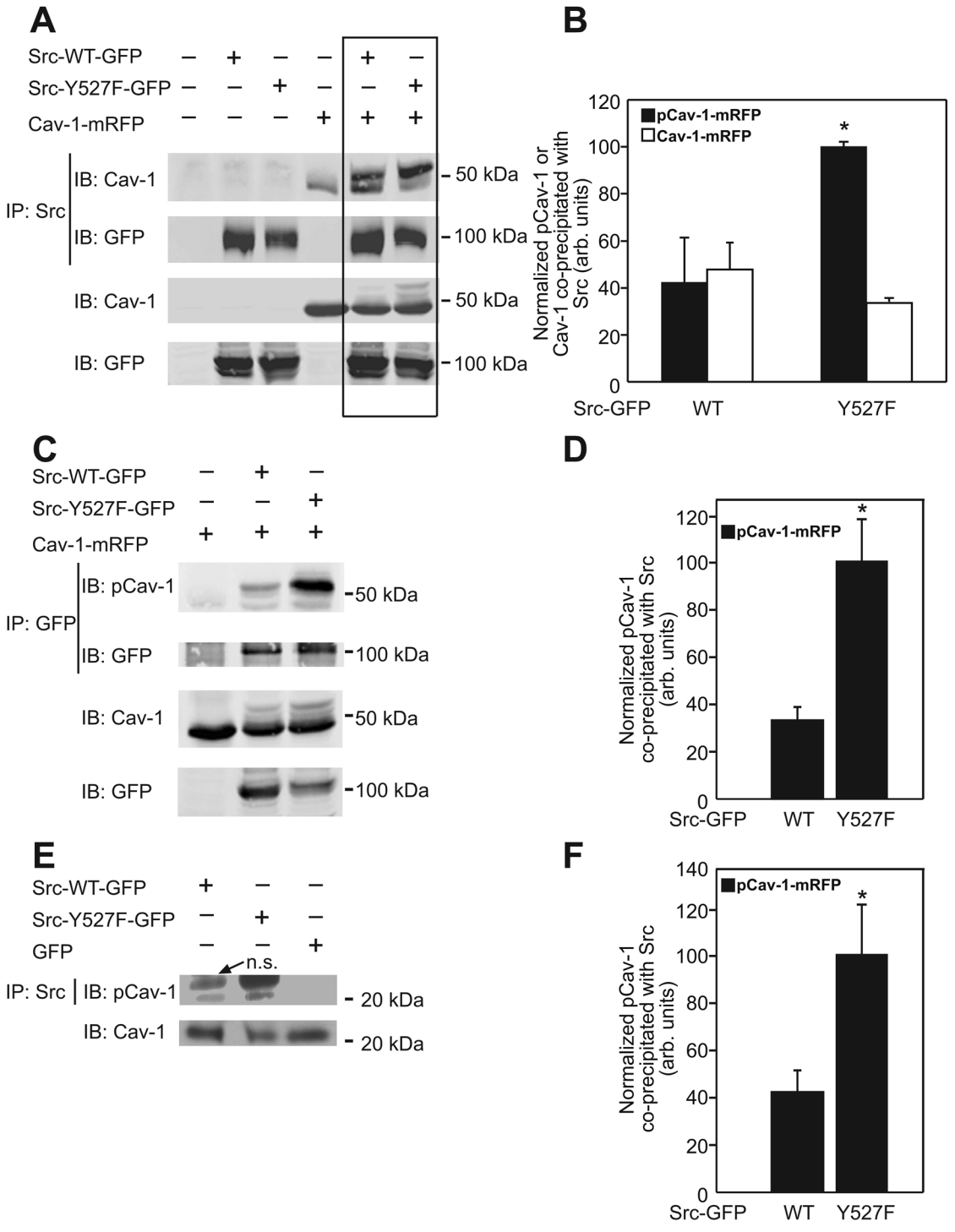

FIGURE 4: pCav-1 coprecipitates preferentially with Src-Y527F–GFP. COS-7 cells in 10-cm dishes were transfected with vectors encoding the indicated proteins (*Materials and Methods*). After 24 h, cells were lysed, and proteins were immunoprecipitated (IP) either with anti-Src (A, E) or anti-GFP (C). The immunoprecipitates were subjected to SDS gel electrophoresis (8.5% polyacrylamide, except in E, for which 12% gels were used) and immunoblotted (IB) using anti–Cav-1, anti–pCav-1, or anti-GFP antibodies. In A (top), pCav-1 was identified as the upper band in the Cav-1 doublet. The lower panels in A, C, and E demonstrate that the expression levels of Cav-1–mRFP or Src-GFP were similar under the different transfection combinations used (blotting control for whole lysates). In E, n.s. designates a nonspecific band coprecipitated with Src-GFP; note that in lane 3, the cells are transfected with GFP rather than with Src-GFP, and therefore the n.s. band does not appear. (B, D, F) Quantification by densitometry (means ± SEM, $n = 3$). Data are presented as coprecipitated pCav-1 (or Cav-1) levels normalized to the levels of immunoprecipitated Src-GFP in each sample, taking the value of pCav-1 coprecipitated with Src-Y527F-GFP as 100%. These experiments reveal a 2.5-fold higher coimmunoprecipitation of pCav-1–mRFP with Src-Y527F relative to Src-WT (B, D). This result was reproduced for endogenous Cav-1 (E, F). Asterisks indicate a significant difference between the pCav-1 levels coprecipitated with Src-Y527F relative to Src-WT (*$p < 0.02$, Student's *t* test).

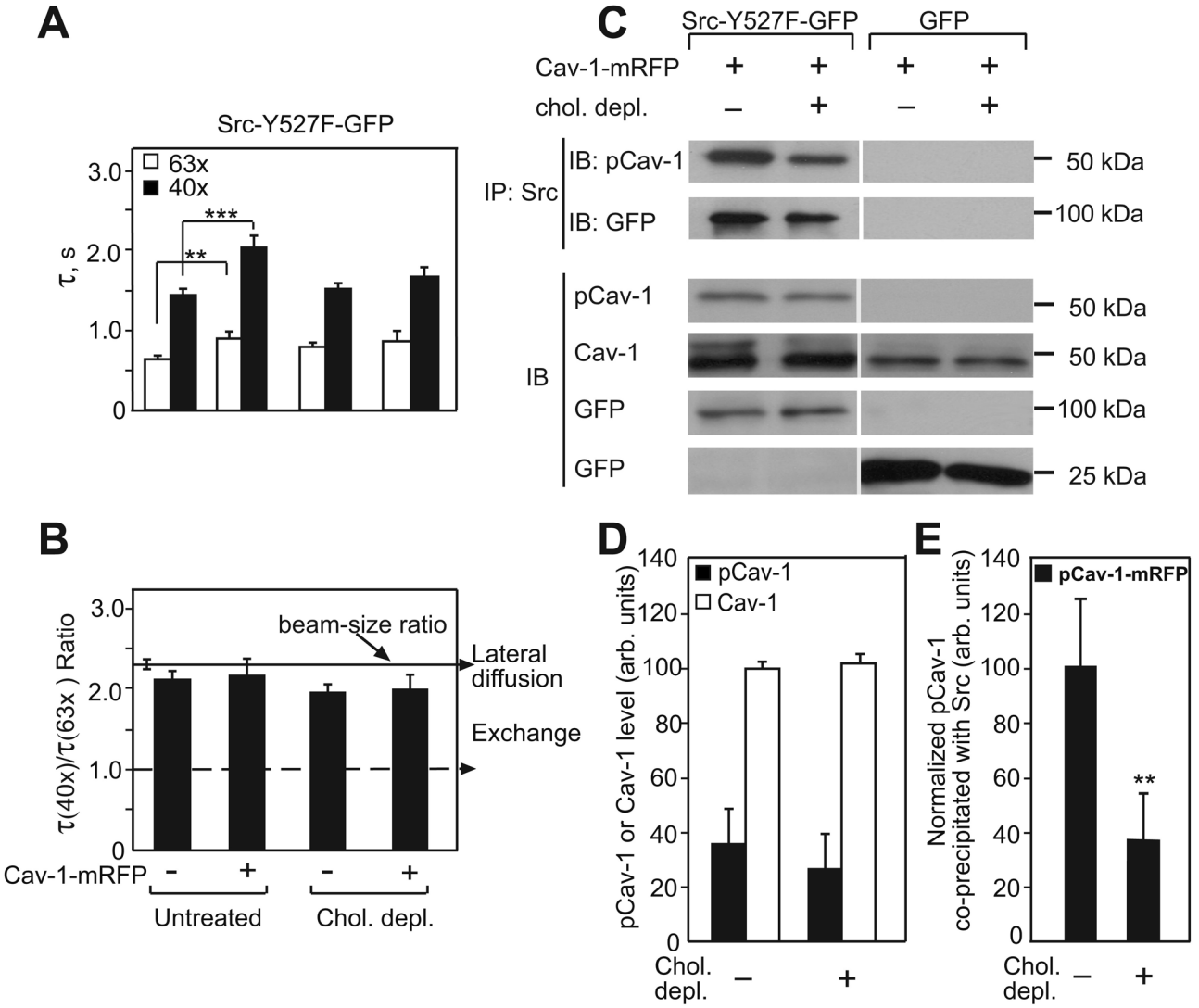

FIGURE 5: The interactions of activated Src with Cav-1 are cholesterol dependent. (A, B) COS-7 cells were transfected and subjected to FRAP beam-size analysis as in Figure 2. FRAP beam-size analysis experiments were conducted with the 63× and 40× objectives as described in the legend to Figure 2, either on untreated cells or on cells subjected to metabolic inhibition of cholesterol synthesis. Bars, means ± SEM of 30–60 measurements. (A) τ values. Before cholesterol depletion, the τ(40×) and τ(63×) values of Src-Y527F were significantly reduced by Cav-1 expression (**$p < 2 \times 10^{-5}$; ***$p < 10^{-7}$). Cholesterol depletion eliminated the Cav-1–mediated retardation in the lateral diffusion rate of Src-Y527F-GFP. (B) τ(40×)/τ(63×) ratios. No significant effects of cholesterol depletion were observed. (C–E) Western blot and coimmunoprecipitation show reduced interactions between activated Src and pCav-1 after cholesterol depletion. COS-7 cells in 10-cm dishes were transfected with expression vectors encoding Cav-1–mRFP together with Src-Y527F-GFP or GFP (control) as described under *Materials and Methods*. At 24 h posttransfection, cells were lysed and subjected either to immunoblotting (IB) with anti–pCav-1, anti-Cav-1 (to determine total Cav-1), or anti-GFP (transfection control) or to immunoprecipitation (IP) with anti-Src, followed by blotting with anti–pCav-1 or anti-GFP as in Figure 4. The levels of pCav-1 and Cav-1 were normalized for transfection efficiency according to the Src-GFP expression level in each sample, assigning the normalized level of Cav-1 in the untreated sample the value of 100%. Neither pCav-1 nor Cav-1 level was significantly altered by cholesterol depletion (C, D). On the other hand, cholesterol depletion significantly reduced the level of pCav-1 coprecipitated with Src-Y527F-GFP (C, E; **$p < 0.01$). These findings indicate that the effects of cholesterol depletion on Src-Y527F-GFP FRAP rates in A and B are due to modulation of interactions between activated Src and Cav-1.

Src-Y527F lateral diffusion. On the other hand, overexpression of Cav-1–C156S, a Cav-1 mutant that lacks the Cys156 palmitoylation site, was as effective as Cav-1 in decreasing Src-Y527F mobility. These findings were corroborated by the results of coimmunoprecipitation studies (Figure 7, C and D), which showed that the Y14F mutation in Cav-1 abolished its coprecipitation with Src, whereas Cav-1–C156S was coprecipitated with high efficiency. Taken together, these results suggest that Cav-1 phosphorylation at Tyr14 is essential for its association with activated Src, whereas the Cys156 palmitoylation site is dispensable for these interactions.

The dependence of Src–Cav-1 interactions on Cav-1 Tyr-14 and on Src kinase activity and SH2 domain function suggests that these

interactions may involve direct binding of the Src SH2 domain to the pTyr residue at position 14 on Cav-1. To test this possibility, we performed far-Western blot experiments (Machida *et al.*, 2007) to examine the binding of fusion proteins of glutathione *S*-transferase (GST) with the Src SH2 domain (GST-SH2) or with a mutated inactive SH2 domain (GST-SH2-R175A) to immunoprecipitated pCav-1 (Figure 8A). The results clearly demonstrate binding of GST-SH2, but not GST-SH2-R175A or GST, to pCav-1. The specificity of the assay is further demonstrated by the lack of GST-SH2 binding to blots derived from cells coexpressing Src-Y527F-GFP together with Cav-1–Y14F–mRFP (Figure 8B). Moreover, the same assay confirmed that the Src SH2 domain can effectively bind the Cav-1–C156S mutant (Figure 8B).

Phosphorylation of Cav-1 by Src enhances the targeting of activated Src to focal adhesions

Cbp, a raft-associated protein that serves as an SFK phosphorylation target, was shown to bind the SH2 domain of activated Src, thus recruiting the latter to rafts/caveolae; the elevated confinement of activated SFKs to rafts/caveolae by Cbp was also reported to suppress SFK-mediated cell transformation (Oneyama *et al.*, 2008, 2009; Resh, 2008). Our novel finding that Src-mediated phosphorylation of Cav-1 at Tyr14 is followed by the binding of Src (via its SH2 domain) to pCav-1 raised the possibility that Cav-1, which resembles Cbp in being a Src phosphorylation target and in its ability to recruit Csk (Glenney and Zokas, 1989; Li *et al.*, 1996b; Cao *et al.*, 2002), might attenuate the targeting of activated Src to FAs in the same way as does Cbp. However, pCav-1 was also reported to be enriched at or near FAs (Lee *et al.*, 2000; del Pozo *et al.*, 2005; Gaus *et al.*, 2006); although studies on pCav-1 localization by fluorescence microscopy are complicated by the cross-reactivity of anti–pY14-Cav-1 with phosphopaxillin (Hill *et al.*, 2007), biochemical evidence links pCav-1 to integrin engagement and FA signaling (Wary *et al.*, 1998; Volonte *et al.*, 2001; del Pozo *et al.*, 2005; Radel and Rizzo, 2005; Gaus *et al.*, 2006), suggesting that pCav-1 might instead have an opposite effect to that of Cbp and enhance the targeting of activated Src to FAs. To distinguish between these possibilities, we conducted quantitative imaging studies to investigate the effects of Cav-1 expression on the targeting of activated Src-GFP to FAs. The experiments used REF52 cells growing on fibronectin-coated coverslips, which display very clear FAs (Figure 9). The cells were cotransfected with Src-Y527F-GFP alone or together with Cav-1–mRFP (WT or Y14F); after 24 h, they were fixed/permeabilized, labeled with anti-paxillin, and subjected to three-dimensional confocal imaging (see *Materials and Methods*). Western blot analysis (Figure 9A) showed that the expression levels of Src-Y527F-GFP and Cav-1–mRFP (WT or Y14F) in all samples were similar. Cells expressing (or not expressing) Cav-1–mRFP were identified by the mRFP fluorescence. On each individual cell, the FA regions were detected by the concentrated paxillin immunolabeling; these regions were segmented and marked by SlideBook (see *Materials and Methods*). The total Src-GFP fluorescence in these marked pixels was divided by the paxillin fluorescence in the same region to obtain a calibrated measure of FA-associated Src-GFP in individual cells. For statistical analysis, we calculated the mean ± SEM of the Src-GFP/paxillin fluorescence intensity ratios from 50–70 cells in each condition. The results (Figure 9) clearly demonstrate that the effect of Cav-1 coexpression is opposite of that reported for Cbp: overexpression of Cav-1–WT but not Cav-1–Y14F with constitutively active Src leads to enrichment of the activated Src in FAs. The failure of Cav-1–Y14F to target activated Src to FAs suggests a requirement for phosphorylation of Cav-1 at Tyr-14 for this effect.

DISCUSSION

There is evidence that Src–membrane interactions are crucial for its signaling and may play an important role in directing active Src to defined cellular regions (Kamps *et al.*, 1985; Buss *et al.*, 1986; Resh, 1999, 2006, 2008; Shvartsman *et al.*, 2007; Oneyama *et al.*, 2008). Although phosphorylation of Cav-1 by Src was reported to be involved in multiple cellular functions, different conclusions were reached on the interdependence of pCav-1 formation and Src localization and activity (Lee *et al.*, 2000; Cao *et al.*, 2002; del Pozo *et al.*, 2005; Gaus *et al.*, 2006; Grande-Garcia *et al.*, 2007; Hill *et al.*, 2007; Joshi *et al.*, 2008; Urra *et al.*, 2012), and the nature of Src–Cav-1 interactions remained unclear (Li *et al.*, 1996b; Lee *et al.*, 2001; Oneyama *et al.*, 2008; Resh, 2008). In the present study we demonstrate that Src displays dynamic interactions with the plasma membrane, which are enhanced and stabilized by Cav-1. We show that the mechanism involves the initial phosphorylation of Cav-1 at Tyr14 by Src, which is followed by binding of the SH2 domain of activated Src to pY14–Cav-1. These interactions promote localization of activated Src to FAs, the dynamics and function of which are known to be regulated by Src (Cary *et al.*, 1996; Wary *et al.*, 1998; Webb *et al.*, 2004; Radel and Rizzo, 2005; Mitra and Schlaepfer, 2006; Yeo *et al.*, 2006).

We formerly used FRAP beam-size analysis to demonstrate that the association of Src with the plasma membrane is regulated by an autocatalytic process in which the phosphorylation of multiple membrane protein targets by Src is followed by enhanced binding of activated Src to the pTyr sites via its SH2 domain (Shvartsman *et al.*, 2007). In accord with these findings, the recovery of Src-WT-GFP in FRAP beam-size experiments was characterized by a mixture of lateral diffusion (with a lipid-like *D* value) and exchange, suggesting relatively weak membrane interactions (Figures 1 and 2). On the other hand, constitutively active Src-Y527F-GFP recovered by pure lateral diffusion (i.e., its exchange rate was significantly slower) and with a smaller *D*, suggesting stabilized membrane association due to binding to membrane proteins that diffuse more slowly (Figures 1 and 2; Shvartsman *et al.*, 2007). Although these findings indicate that Src–membrane association is regulated by its activity and interactions with membrane protein targets, the biological implications of these interactions remained unclear. To explore these issues in the context of Cav-1, a well-known Src target protein, we conducted FRAP beam-size analysis on Src-WT-GFP and Src-Y527F-GFP in cells coexpressing Cav-1–mRFP. Of note, Cav-1 markedly reduced the lateral diffusion rate of Src-Y527F-GFP but had no effect on the FRAP rates of unactivated Src-WT-GFP after serum starvation (Figure 2, C and D). The dependence of the Src–Cav-1 interactions on Src activity is further exemplified by the partial retardation of the lateral diffusion of Src-WT by PDGF in cells coexpressing Cav-1 (Figure 2C), most likely reflecting activation of a portion of the Src population. Moreover, the retarding effects of Cav-1 on the lateral diffusion of activated Src are cholesterol dependent (Figure 5) and accompanied by reduced association of activated Src with pCav-1, as shown by coimmunoprecipitation (Figure 5E). The notion that Src–Cav-1 interactions require Src activity was validated by the highly preferential coimmunoprecipitation of Cav-1 with constitutively active Src versus Src-WT (Figure 4). Given that Cav-1 is an established Src phosphorylation target, the requirement for Src activity is consistent with the selective coprecipitation of pCav-1, which migrates at a higher molecular weight relative to unphosphorylated Cav-1 (Figure 4).

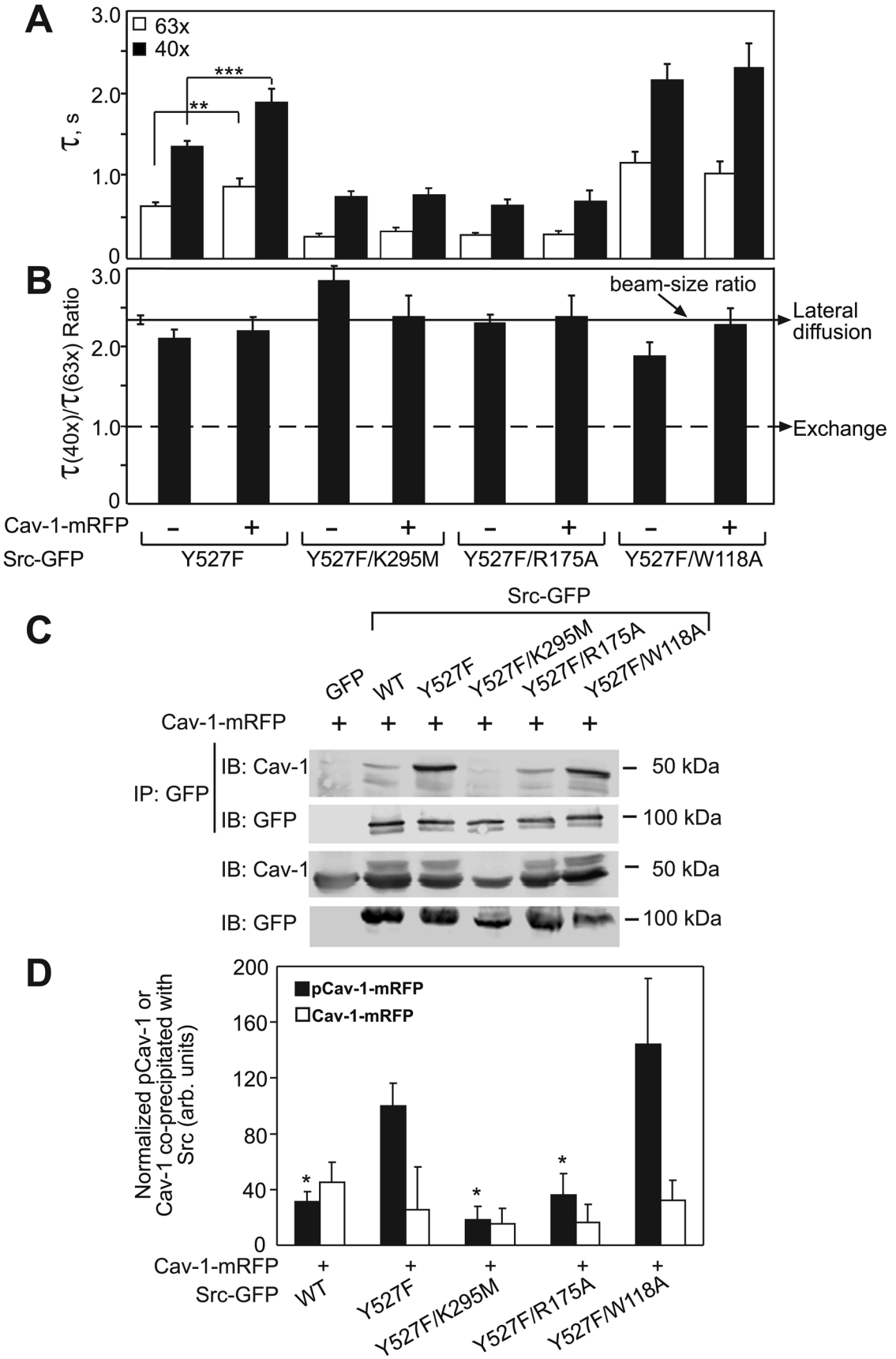

FIGURE 6: The effects of Cav-1 on Src–membrane interactions depend on the Src SH2 domain and kinase activity. COS-7 cells were cotransfected with a vector encoding a Src-GFP derivative together with a Cav-1–mRFP–encoding vector or empty vector (see *Materials and Methods*). FRAP beam-size analysis studies were conducted as in

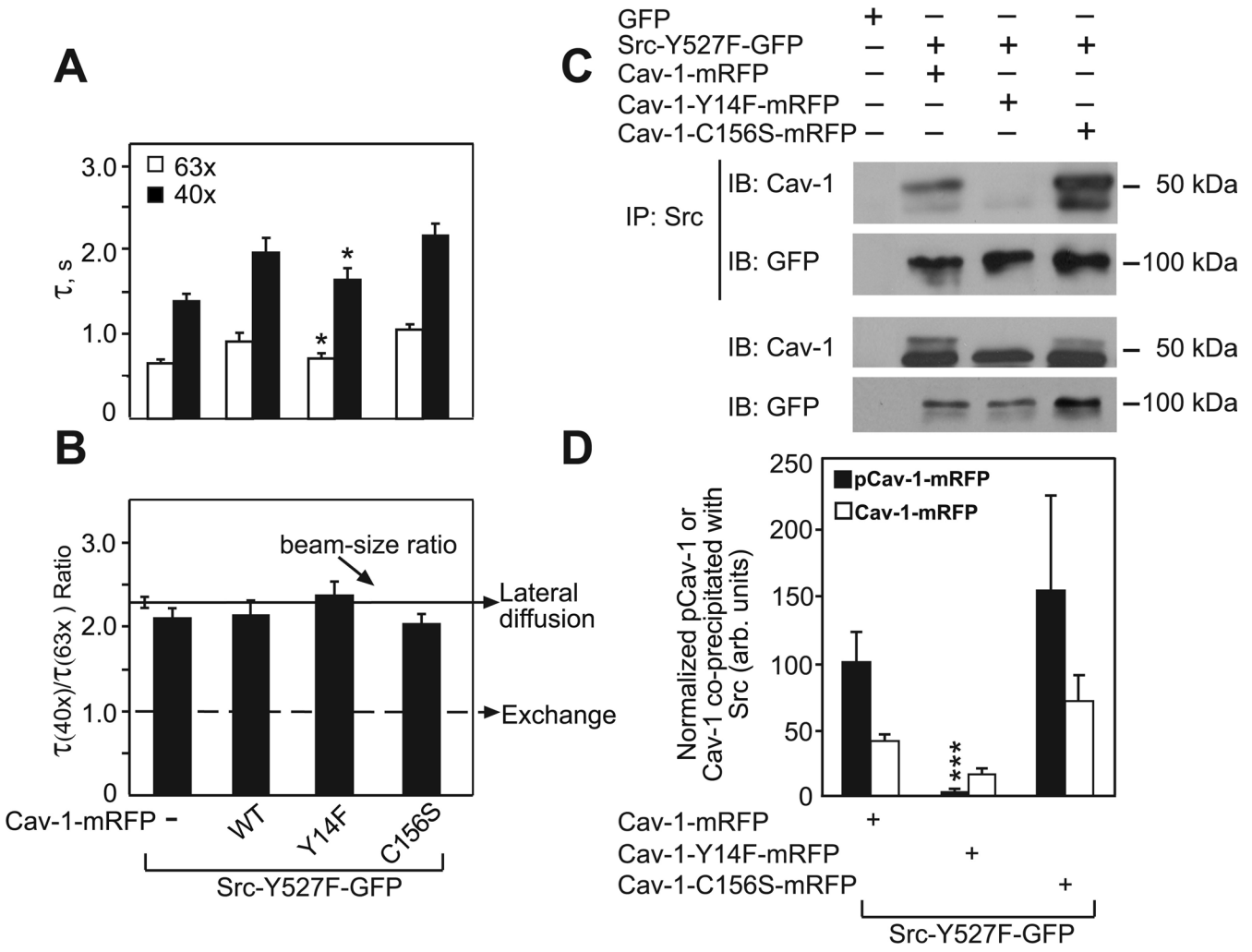

FIGURE 7: Phosphorylation of Cav-1 on Tyr-14 is required for its interaction with Src-Y525F. COS-7 cells were cotransfected with Src-Y527F-GFP together with a Cav-1–mRFP derivative (WT, Y14F, or C156S; see *Materials and Methods*). FRAP beam-size analysis was performed as in Figure 2. Immunoprecipitation (IP) and immunoblotting (IB) studies were performed as in Figure 4A, blotting with anti–Cav-1 or anti-GFP. (A) τ values. Bars, means ± SEM of 30–60 measurements. Comparison of the effects of coexpression of Cav-1 mutants (Cav-1–Y14F or Cav-1–C156S) with those of Cav-1–WT on the τ(63×) or τ(40×) values of Src-Y527F-GFP shows that only Cav-1–Y14F has significantly reduced effects (*$p < 0.01$; Student's t test). (B) τ(40×)/τ(63×) ratios. No significant differences were observed. (C, D) Coimmunoprecipitation studies. (C) A typical experiment; (D) quantification ($n = 3$). Data normalization and presentation are as in Figure 4A. In accord with the FRAP studies, no pCav-1 (upper band in the Cav-1 doublet; C) coprecipitation with Src-Y527F-GFP was observed for the Y14F Cav-1 mutant, indicating that the coprecipitation requires phosphorylation of Tyr-14 (***$p < 10^{-10}$). The expression levels of the Cav-1-mRFP mutants and of Src-GFP were similar in all cases (bottom two panels in C).

Figure 2. Immunoprecipitation (IP) and immunoblotting (IB) studies were performed as in Figure 4C, blotting with anti–Cav-1 or anti-GFP. (A) FRAP τ values. Bars, means ± SEM of 30–60 measurements. Only the τ values of Src-Y527F-GFP are significantly retarded by Cav-1–mRFP expression (**$p < 2 \times 10^{-5}$; ***$p < 10^{-7}$). Thus the ability of Cav-1 to retard the lateral diffusion of Src-GFP requires Src kinase activity and SH2-domain binding. For Src-Y527F/W118A, the effect of Cav-1 is masked by the enhanced membrane interactions of the SH3-defective Src mutant (see the text). (B) τ(40×)/τ(63×) ratios. Bootstrap analysis does not show significant effects on the τ ratios of any of the Src-GFP mutants upon cotransfection with Cav-1-mRFP (the minor increase in the τ ratio of Src-Y527F/W118A upon coexpression of Cav-1 is not significant). (C, D) Coimmunoprecipitation experiments. (C) A typical experiment; (D) quantification of three experiments by densitometry. Data are presented as pCav-1 (upper band in the doublet around 50 kDa) or Cav-1 (lower band) normalized to the levels of immunoprecipitated Src-GFP in each sample, taking the value of pCav-1 coprecipitated with Src-Y527F-GFP as 100%. The amounts of pCav-1 coprecipitated with kinase-dead Src-Y527F/K295M or SH2-defective Src-Y527F/R175A were significantly lower relative to Src-Y527F (*$p < 0.02$); a similar phenomenon was obtained with unactivated Src-WT. The expression levels of Cav-1–mRFP and Src-GFP were similar under the different transfection combinations used (see two lower IB strips in C).

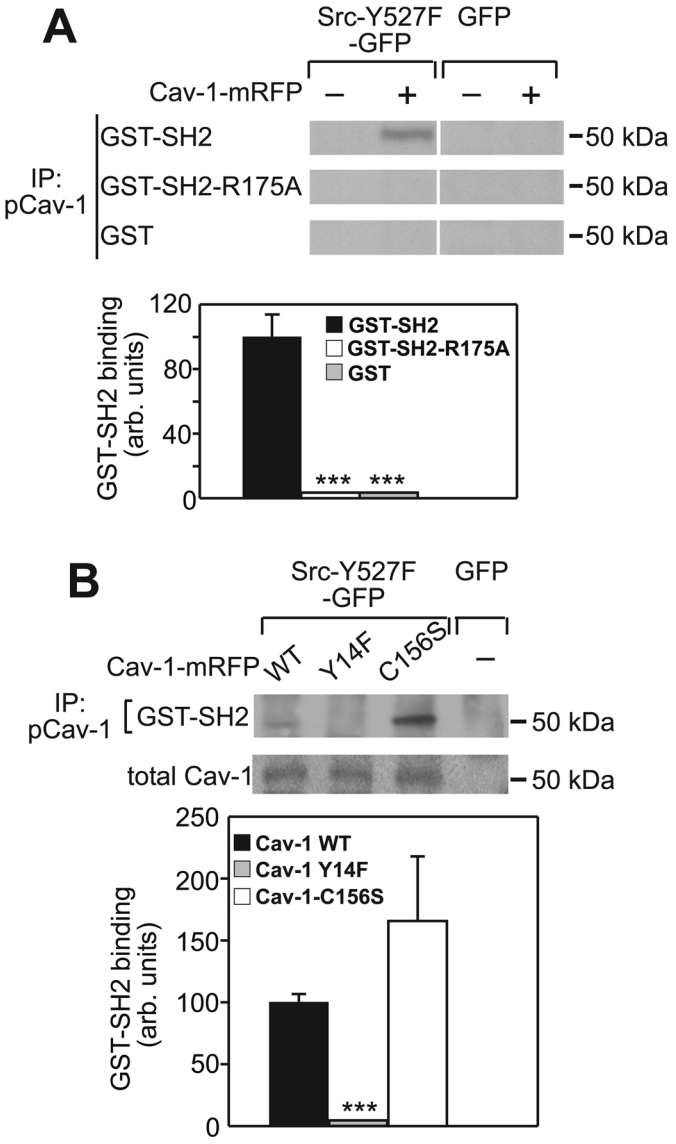

FIGURE 8: The Src SH2 domain can bind directly to p-Y14–Cav-1. COS-7 cells were transfected with vectors encoding the indicated proteins, lysed, and subjected to immunoprecipitation with anti–pCav-1, followed by SDS–PAGE and blotting as described under *Materials and Methods*. The blots were probed with GST fusion proteins, followed by rabbit anti-GST and peroxidase–goat anti-rabbit antibodies (*Materials and Methods*). For quantification, three independent experiments were subjected to densitometric analysis, taking the GST-SH2 labeling signal of the pCav-1 band obtained for Cav-1–mRFP coexpressed with Src-Y527F-GFP as 100%. (A) The Src SH2 domain binds to pCav-1 in far-Western blotting. The pCav-1 band is labeled by GST-SH2 but not by GST-SH2-R175A or GST alone. In the GFP-transfected samples, very little pCav-1 is present, resulting in negligible GST-SH2 binding. Asterisks indicate significant differences from GST-SH2 binding (***$p < 10^{-10}$). (B) GST-SH2 binding requires phosphorylation of Cav-1 on Tyr-14. Far-Western labeling with GST-SH2 was observed for cells cotransfected with constitutively active Src and Cav-1–WT or Cav-1–C156S but not with Cav-1–Y14F (***$P < 10^{-10}$ relative to GST-SH2 binding in cells transfected with Cav-1 WT). The expression levels of total Cav-1 were similar (see total Cav-1 immunoblot, bottom).

The dependence on Src kinase activity is also demonstrated by the failure of Cav-1 to retard the lateral diffusion of activated Src bearing a mutation that abrogates its kinase activity (Src-Y527F/K295M; Figure 6, A and B), as well as the lack of Cav-1 coprecipitation with this mutant (Figure 6, C and D). Moreover, in cells expressing the kinase-dead Src-Y527F mutant, no pCav-1 was detected already in the lysate (Figure 6C, Cav-1 immunoblot panel), suggesting that Cav-1 phosphorylation is mediated primarily by the kinase activity of the transfected Src. In addition to the kinase activity of Src, the integrity of the Src SH2 domain is required for both Src–Cav-1 interactions and the Cav-1–mediated effects on Src-Y527F mobility, as both were impaired in the Src-Y527F/R175A mutant (Figure 6). In contrast, the SH3 domain appears to be dispensable for Src–Cav-1 interactions (Figure 6).

The foregoing findings are in accord with a role for Src SH2 domain–pTyr interactions in regulating Src–Cav-1 association. To directly assess this hypothesis, we mutated the Src phosphorylation target residue on Cav-1 (Tyr-14). In accord with all the foregoing results, Cav-1–Y14F failed to interact with Src-Y527F both in the lateral diffusion FRAP assay and in coimmunoprecipitation studies (Figure 7). Of note, mutation of Cav-1 to eliminate the palmitoylation site at Cys-156 (Cav-1–C156S) did not reduce its association with Src-Y527F as measured by either FRAP or coimmunoprecipitation (Figure 7). These results are in contrast with an earlier report that Cys-156 is important for Src-mediated Cav-1 phosphorylation (Lee *et al.*, 2001) and are in good agreement with a role for interactions between the Src SH2 domain and pTyr-proteins (such as pTyr-Cbp) in the recruitment of activated Src to caveolae (Oneyama *et al.*, 2008, 2009; Resh, 2008). Strong support for the notion that the Src SH2 domain binds directly to pY14 on Cav-1 (as well as to Cav-1-C156S, but not to Cav-1-Y14F) is provided by far-Western studies (Figure 8) demonstrating the interaction of pCav-1 with the WT GST-SH2 of Src but not with GST-SH2-R175A (defective Src-SH2 mutant).

In view of the conflicting reports on the cellular localization of pCav-1 in FAs (Lee *et al.*, 2000; del Pozo *et al.*, 2005; Gaus *et al.*, 2006; Hill *et al.*, 2007), we investigated the effects of Cav-1 overexpression on the localization of Src-Y527F-GFP in FAs. Our quantitative imaging studies (Figure 9) demonstrate that Cav-1, but not Cav-1–Y14F, enhances the localization of activated Src in FAs. These findings are in line with earlier biochemical studies, which reported pCav-1 to be involved in integrin engagement and FA signaling (Wary *et al.*, 1998; Volonte *et al.*, 2001; del Pozo *et al.*, 2005; Radel and Rizzo, 2005; Gaus *et al.*, 2006).

On the basis of the results described, we propose a mechanism in which the initial binding of Src to Cav-1 throughout the plasma membrane (where Cav-1 is enriched in caveolae) is followed by phosphorylation of Cav-1 at Tyr-14 by Src. The SH2 domain of active Src (in the open conformation) subsequently binds directly and tightly to the pY14 residue on Cav-1 and follows the latter to FA regions. This results in enrichment of FAs in Src activity, which potentially affects FA dynamics and cell–matrix interactions (Cary *et al.*, 1996; Webb *et al.*, 2004; Radel and Rizzo, 2005; Mitra and Schlaepfer, 2006; Yeo *et al.*, 2006). This is a novel function for Cav-1, which may have implications for Src-mediated regulation of metastasis.

MATERIALS AND METHODS

Reagents

Rabbit antibodies to Cav-1 (N-20), pCav-1 (Tyr 14; sc-101653), and GFP (FL) were obtained from Santa Cruz Biotechnology

(Santa Cruz, CA). Mouse anti-GFPs (B-2) from Santa Cruz Biotechnology and Abcam (Cambridge, UK; ab1218) were used for blotting and immunoprecipitation, respectively. Mouse anti–pCav-1 (Tyr-14; clone 56) and anti-paxillin were from BD Transduction Laboratories (San Jose, CA). Mouse anti-Src (clone GD11) was from Millipore (Billerica, MA). Rabbit anti-GST was from Sigma (St. Louis, MO). Mouse anti–β-actin was from MP Biomedicals (Solon, OH). Peroxidase-conjugated goat anti-rabbit and anti-mouse immunoglobulin Gs (IgGs) were from Jackson ImmunoResearch Laboratories (West Grove, PA). Alexa 647–goat anti-mouse IgG was from Invitrogen-Molecular Probes (Eugene, OR). PDGF (rhPDGF-BB) was from R&D Systems, and fibronectin was from Biological Industries (Beit Haemek, Israel). Protease inhibitor cocktail (P8340) was from Sigma.

Plasmids

Biologically active pEGFP-N1 vectors for Src-WT-GFP and Src-Y527F-GFP (chicken c-Src; Sandilands *et al.*, 2004) were donated by M. C. Frame (University of Edinburgh, Edinburgh, United Kingdom). Src-Y527F-GFP served as template to prepare open-conformation double mutants (kinase-dead Src-Y527F/K295M-GFP, SH2-inactivated Src-Y527F/R175A-GFP, and SH3-defective Src-Y527F/W118A-GFP), as previously described (Shvartsman *et al.*, 2007). Canine Cav-1–mRFP in pcDNA3.1 (+) (Sharma *et al.*, 2004) was donated by R. E. Pagano (Mayo Clinic, Rochester, MN). This vector served as template to generate Cav-1–Y14F–mRFP or Cav-1–C156S–mRFP mutants by site-directed mutagenesis using QuikChange (Stratagene). The primers used were 5′-GGGGCACCTCTTCACCGTTCCCATCCG-3′ (forward) and 5′-CGGATGGGAACGGTGAAGAGGTGCCCC-3′ (reverse) for the Y14F mutation (underlined); or 5′-CGTCCACACCTTCTCTGACCCGTTCTTTGAGGC-3′ (forward) and 5′-GCCTCAAAG-AACGGGTCAGAGAAGGTGTGGACG-3′ (reverse) for the C156S mutation (underlined).

Cell culture and transfections

COS-7 and REF52 cells (American Type Culture Collection) were grown in DMEM containing 10% fetal calf serum (FCS) as described (Shvartsman *et al.*, 2003; Wolfenson *et al.*, 2009) on glass coverslips (uncoated or precoated with 20 µg/ml fibronectin) placed in six-well plates (for FRAP and imaging studies) or on 10-cm dishes (for biochemical experiments). COS-7 cells were cotransfected using DEAE-dextran (Sigma; Seed and Aruffo, 1987) with a vector encoding a Src-GFP derivative (0.15 µg of DNA; replaced by pEGFP-N1 in some biochemical control experiments) together with Cav-1–mRFP (WT or mutant; 0.3 µg) or empty pcDNA3.1 vector (control). REF52 cells were cotransfected by TransIT-LT1 (Mirus, Madison, WI) with the same vector combinations, using twofold higher DNA quantities.

siRNA-mediated expression knockdown experiments

COS-7 cells were grown on six-well plates (for biochemical experiments) or glass coverslips placed in six-well plates (for FRAP studies). They were cotransfected by jetPRIME (Polyplus, Illkirch, France) with a vector encoding Src-Y527F-GFP (0.15 µg) together with 50 nM ON-TARGETplus human Cav-1 SMART pool siRNA (Dharmacon, Lafayette, CO), target sequences CUAAACACCUCAACGAUGA, GCAAAUACGUAGACUCGGA, GCAGUUGUACCAUGCAUUA, and GCAUCAACUUGCAGAAAGA; or with 50 nM ON-TARGETplus nontargeting pool siRNA (Dharmacon; negative control). Immunoblotting analysis or FRAP studies were performed 48 h posttransfection as described in the relevant subsequent sections.

Cholesterol depletion

At 6 h posttransfection, COS-7 cells were subjected in some experiments (see figure legends) to metabolic cholesterol depletion by incubation (18 h) with 50 µM compactin and 50 µM mevalonate (both from Sigma) in medium supplemented with 10% lipoprotein-deficient fetal calf serum following established procedures (Lin *et al.*, 1998; Shvartsman *et al.*, 2006). To assay the cholesterol content of the treated cells, they were homogenized, and the membrane fraction was isolated by centrifugation as described earlier (Shvartsman *et al.*, 2006). The cholesterol content in the membrane fraction was measured using the F-CHOL kit (Boehringer, Ingelheim, Germany) according to manufacturer's instructions. This assay yielded a 31 ± 2% reduction in the cholesterol level relative to untreated cells ($n = 5$). We showed (Eisenberg *et al.*, 2006; Shvartsman *et al.*, 2006) that this treatment selectively increases the lateral diffusion of raft-associated proteins but does not affect the general biophysical properties of the plasma membrane, as shown by the lack of effect on the FRAP dynamics of nonraft proteins.

FRAP

COS-7 cells expressing Src-GFP proteins (alone or together with a Cav-1–mRFP mutant) were taken for FRAP studies 24 h after transfection. Measurements were in Hank's balanced salt solution supplemented with 20 mM 4-(2-hydroxyethyl)-1-piperazineethanesulfonic acid (HEPES), pH 7.2. In some experiments, cells were first subjected to metabolic cholesterol depletion or to serum starvation in medium containing 0.5% serum (16 h, initiated at 6 h posttransfection), followed by 1 h in serum-free medium and a 10-min incubation at 37°C with or without 50 ng/ml PDGF. To minimize internalization, FRAP measurements were at 22°C, replacing samples within 15 min. An argon ion laser beam (Innova 70C; Coherent, Santa Clara, CA) was focused through a fluorescence microscope (AxioImager.D1; Carl Zeiss MicroImaging, Jena, Germany) to a spot with $\omega = 0.77 \pm 0.03$ µm (Plan Apochromat 63×/1.4 numerical aperture [NA] oil-immersion objective) or 1.17 ± 0.05 µm (C Apochromat 40×/1.2 NA water-immersion objective), and experiments were conducted with each (beam-size analysis; Henis *et al.*, 2006). The ratio between the bleached areas was 2.28 ± 0.17 ($n = 59$). After a brief measurement at monitoring intensity (488 nm, 1 µW), a 5-mW pulse (5–10 ms) bleached 60–75% of the fluorescence in the spot, and recovery was followed by the monitoring beam. The characteristic fluorescence recovery time (τ) and mobile fraction (R_f) were extracted from the FRAP curves by nonlinear regression analysis, fitting to a lateral diffusion process (Henis *et al.*, 2006). The R_f values for all Src-GFP proteins were >0.90 in all cases.

Statistical analysis of FRAP data

The significance of differences between τ values measured with the same beam size was evaluated by Student's *t* test. To compare ratio measurements—that is, $\tau(40\times)/\tau(63\times)$ and $\omega^2(40\times)/\omega^2(63\times)$ (see *Results*)—we used bootstrap analysis, which is preferable for comparison between ratios (Efron and Tibshirani, 1993). The bootstrap analysis was as described earlier (Gutman *et al.*, 2010), using 1000 bootstrap samples.

Imaging data acquisition and processing

REF52 cells growing on fibronectin-coated coverslips were cotransfected (TransIT-LT1) with Src-Y527F-GFP together with Cav-1–mRFP (WT or the Y14F mutant) or empty vector (control). After fixation and permeabilization, cells were labeled with 5 µg/ml mouse anti-paxillin, followed by 10 µg/ml Alexa 647–goat anti-mouse IgG. Images were acquired with a spinning disk (Yokogawa CSU-22 confocal

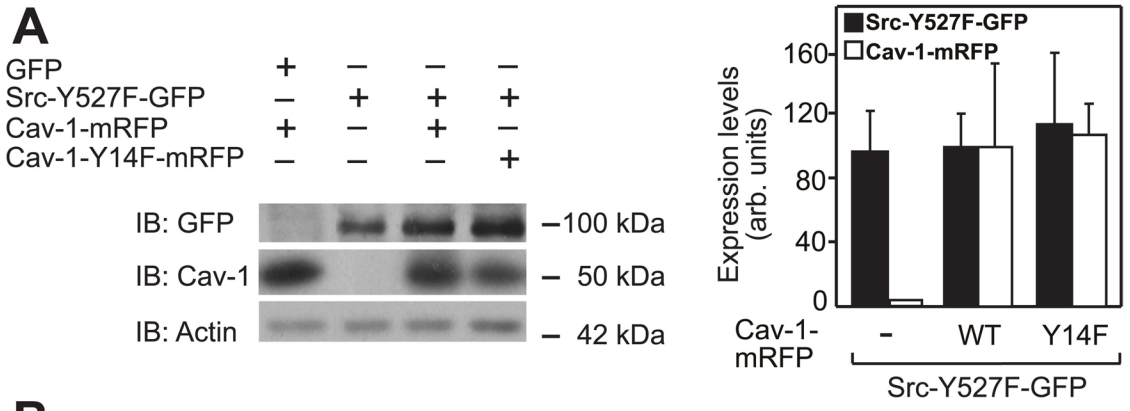
A
GFP + – – –
Src-Y527F-GFP – + + +
Cav-1-mRFP + – + –
Cav-1-Y14F-mRFP – – – +
IB: GFP
IB: Cav-1
IB: Actin
–100 kDa
– 50 kDa
– 42 kDa
Src-Y527F-GFP
Cav-1-mRFP
Expression levels (arb. units)
160
120
80
40
0
Cav-1-mRFP
-
WT
Y14F
Src-Y527F-GFP

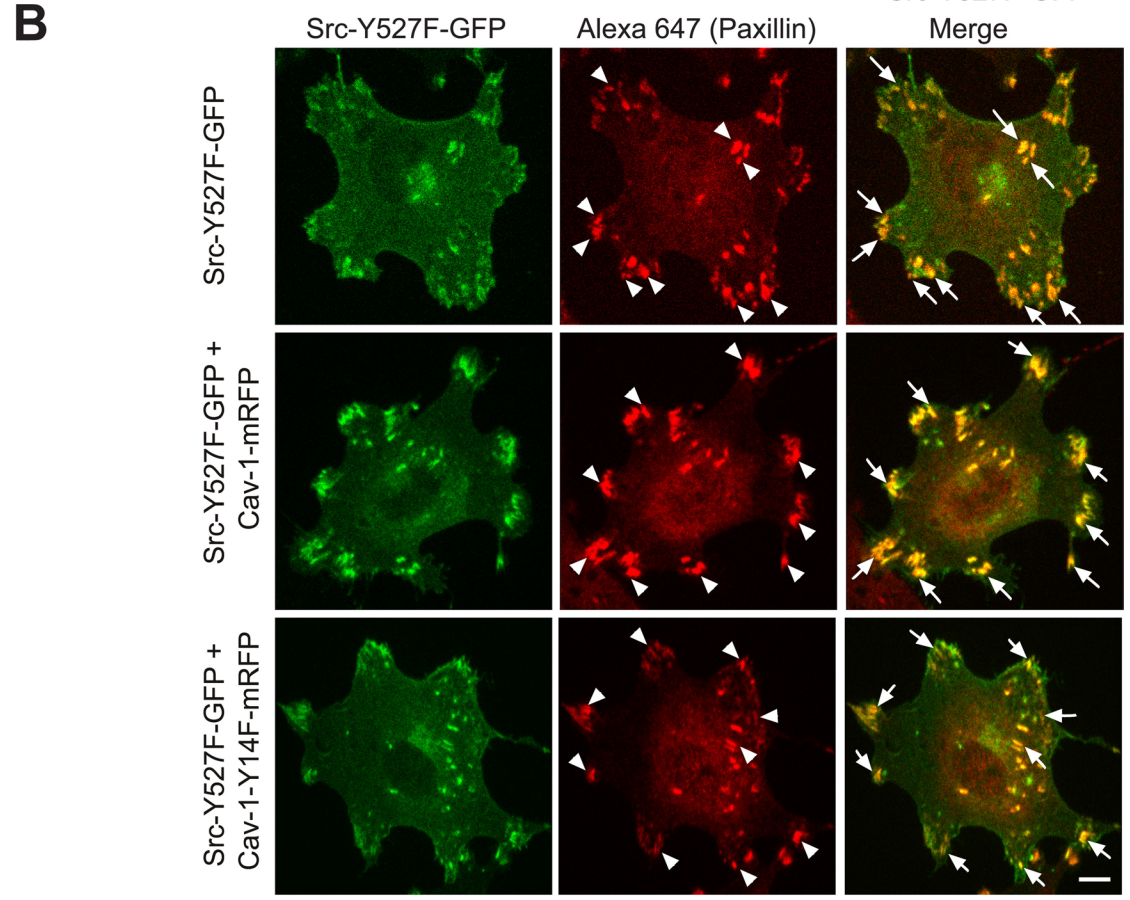
B
Src-Y527F-GFP
Alexa 647 (Paxillin)
Merge
Src-Y527F-GFP
Src-Y527F-GFP + Cav-1-mRFP
Src-Y527F-GFP + Cav-1-Y14F-mRFP

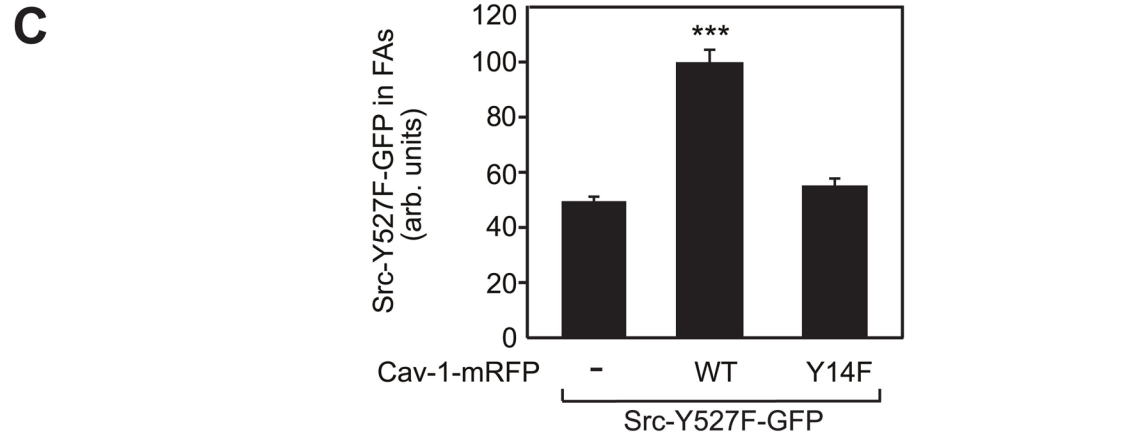
C
Src-Y527F-GFP in FAs (arb. units)
120
100
80
60
40
20
0
***
Cav-1-mRFP
-
WT
Y14F
Src-Y527F-GFP

head) microscope (Axiovert 200M; Carl Zeiss MicroImaging) with a Photometrics (Tucson, AZ) Evolve electron-multiplying charge-coupled device camera, under the control of SlideBook (Intelligent Imaging Innovations, Denver, CO). A 63×/1.4 NA oil immersion objective (Plan Apochromat) was used. Three dimensional (3D) image stacks were generated by sequential acquisition along the *z*-axis by varying the position of a piezoelectrically controlled stage (step size, 0.29 µm). GFP, mRFP, and Alexa 647 were excited with solid-state lasers at 473 nm (50 mW), 561 nm (50 mW), or 660 nm (100 mW), respectively. The image acquisition exposure time was 0.3 s. The 3D images were restored by nearest-neighbor deconvolution (Agard *et al.*, 1989; Chetrit *et al.*, 2009) using SlideBook. Cells expressing (or not expressing) Cav-1–mRFP were identified by the mRFP fluorescence. In each cell group, the FA regions were identified by the concentrated paxillin immunolabeling (using anti-paxillin followed by Alexa 647–goat-anti-mouse IgG). To mark the paxillin-positive pixels in these regions, images were intensity-based segmented with the paxillin-specific channel. The total Src-GFP fluorescence in these marked pixels was divided by the paxillin fluorescence in the same region to obtain a calibrated measure of FA-associated Src-GFP in individual cells. For statistical analysis, the mean ± SEM of the Src-GFP/paxillin fluorescence intensity ratios from 50–70 cells in each condition was calculated.

Immunoblotting and immunoprecipitation

COS-7 cells grown and transfected as described under *Cell culture and transfections* were subjected (or not) to cholesterol depletion, followed by lysis on ice (25 min) with lysis buffer (10 mM Tris, pH 7.5, 50 mM NaCl, 1% Triton X-100, 60 mM octyl glucoside, protease inhibitor cocktail, and 0.1 mM Na_3VO_4; Li *et al.*, 1996b). After low-speed centrifugation to remove nuclei and cell debris, the lysates were subjected to SDS–PAGE (8.5% polyacrylamide) and immunoblotting as described previously (Kfir *et al.*, 2005), loading 10 µg of protein per lane. The blots were cut into two pieces (covering the 50- and 100-kDa regions), which were then probed (12 h, 4°C) by primary antibodies (rabbit anti-Cav-1 or anti–pCav-1 at 1:10,000, rabbit anti-GFP at 1:5000, mouse anti-GFP at 1:500, mouse anti-pTyr at 1:1000, or mouse anti–β-actin at 1:10,000), followed by peroxidase-coupled goat anti-rabbit or anti-mouse IgG (1:10,000 for 1 h at 22°C). Where indicated (see Figure 5), the blots probed for pCav-1 were acid stripped and reprobed with anti–Cav-1 to determine total Cav-1, following the protocol described earlier (Kfir *et al.*, 2005). The bands were visualized by enhanced chemiluminescence (Amersham) and quantified by densitometry (EZQuant-Gel 2.2; EZQuant).

In coimmunoprecipitation experiments, cell lysates were subjected to immunoprecipitation before SDS–PAGE and immunoblotting as described. After taking 10 µg of protein of each lysate to evaluate total Src-GFP or Cav-1–mRFP levels by immunoblotting, we subjected lysates (1 mg protein) to immunoprecipitation of Src-GFP by 2 µg of mouse anti-GFP or 2.5 µg of anti-Src antibodies essentially as described previously (Donaldson *et al.*, 2000; Shvartsman *et al.*, 2007). Alternatively, Cav-1 (2 µg of rabbit anti–Cav-1) or pCav-1 (2 µg of mouse anti-pCav-1) was precipitated. Protein A–Sepharose (for polyclonal antibodies) or Protein G–Sepharose (for mouse antibodies) beads (Sigma) were blocked in HNTG buffer (20 mM HEPES, pH 7.5, 0.15 mM NaCl, 0.1% Triton X-100, 10% glycerol) containing 5% bovine serum albumin for 30 min at 22°C, followed by incubation with the antibodies for 30 min at 22°C. The beads were then incubated with the cell lysates for 2 h at 4°C. The complexes were washed three times in HNTG buffer, and the bound material was solubilized in 30 µl of SDS sample buffer and subjected to SDS–PAGE and immunoblotting as described.

Construction, expression, and purification of GST fusion proteins

Construction of a pGEX-KG plasmid encoding GST fused to the Src SH2 domain (chicken c-Src amino acids 148–251) was previously described (Shvartsman *et al.*, 2007). An analogous construct with an inactivating mutation in SH2, GST-SH2-R175A, was generated similarly, except that Src-Y527F/R175A served as a template for PCR amplification; the *Bam*HI/*Hin*dIII-digested fragment was then recloned into the same sites of the pGEX-KG vector. To express the fusion constructs, transformed bacteria were grown in fresh LB medium for 2 h to A_{550} = 0.5–1. Isopropyl β-D-1-thiogalactopyranoside was then added to 1 mM for an additional 4 h. The bacteria (250 ml) were harvested by centrifugation (5000 × *g*, 15 min, 4°C). Purification of the GST fusion proteins followed established protocols (Sambrook and Russell, 2001).

Far-Western blots

Transfected cells were subjected to lysis, immunoprecipitation with anti–pCav-1, SDS–PAGE. and blotting as described under *Immunoblotting and immunoprecipitation*. For the binding reaction, GST fusion proteins (or GST) were incubated with the blocked membrane in TBST (50 mM Tris, pH 7.5, 150 mM NaCl, 0.1% Tween 20) at a final concentration of 1.5 µg/ml for 1 h at 22°C. After three 10-min washes (22°C) with TBST, the blots were incubated (1 h, 22°C) with anti-GST (1:5000 in TBST), washed three times, and incubated with peroxidase–goat anti-rabbit IgG (1:10,000, 1 h, 22°C). After extensive wash, bound probe was detected by enhanced chemiluminescence and quantified by densitometry.

FIGURE 9: Cav-1 enhances the localization of Src-Y527F in focal adhesions. REF52 cells grown on fibronectin-coated coverslips were cotransfected with Src-Y527F-GFP together with a Cav-1–mRFP derivative (WT or Y14F) or empty vector, fixed/permeabilized, and subjected to immunostaining of paxillin using Alexa 647–conjugated secondary IgG (see *Materials and Methods*). Cells expressing Cav-1–mRFP (WT or Y14F) were identified by mRFP fluorescence. (A) Western blot analysis shows similar Src-Y527F-GFP or Cav-1–mRFP (WT and Y14F) levels under all transfection conditions. (B) Representative images of cells expressing Src-Y527F-GFP without or with a Cav-1–mRFP derivative were imaged using a spinning-disk confocal microscope (*Materials and Methods*). The images depict the fluorescence of Src-GFP and paxillin. Arrowheads point at FAs, identified by paxillin (red) fluorescence; arrows indicate colocalization of Src-Y527F-GFP with paxillin. Bar, 10 µm. (C) Quantification of the fluorescence intensity of Src-GFP in FAs. The 3D images were intensity-based segmented with the paxillin-specific channel, as described in *Materials and Methods*. After marking these pixels, we divided the total Src-GFP fluorescence in these regions by the paxillin fluorescence in the same region, yielding a calibrated measure for the level of Src-GFP associated with FAs. Data are presented as the mean ± SEM of the Src-GFP/paxillin fluorescence intensity ratios from 50–70 cells for each condition, taking the value for Src-Y527F-GFP in FAs in cells expressing Cav-1-mRFP as 100. Asterisks indicated significant differences relative to cells expressing only Src-Y527F-GFP (***$p < 10^{-10}$; Student's *t* test).

ACKNOWLEDGMENTS

We thank M.C. Frame and R. E. Pagano for their generous donation of plasmids. This work was supported by Grant 2007016 from the United States–Israel Binational Science Foundation (to Y.I.H. and G.S.M.), National Institutes of Health Grant CA17542 (to G.S.M.), and a grant from the Israel Cancer Association through the estate of the late Alexander Smidoda (to Y.I.H.). Y.I.H. is an incumbent of the Zalman Weinberg Chair in Cell Biology, Tel Aviv University, Tel Aviv, Israel, and G.S.M. of the Judy C. Webb Chair in Cell and Developmental Biology, University of California, Berkeley, CA.

REFERENCES

Abram CL, Courtneidge SA (2000). Src family tyrosine kinases and growth factor signaling. Exp Cell Res 254, 1–13.

Agard DA, Hiraoka Y, Shaw P, Sedat JW (1989). Fluorescence microscopy in three dimensions. Methods Cell Biol 30, 353–377.

Anderson RG, Jacobson K (2002). A role for lipid shells in targeting proteins to caveolae, rafts, and other lipid domains. Science 296, 1821–1825.

Aoki T, Nomura R, Fujimoto T (1999). Tyrosine phosphorylation of caveolin-1 in the endothelium. Exp Cell Res 253, 629–636.

Bjorge JD, Jakymiw A, Fujita DJ (2000). Selected glimpses into the activation and function of Src kinase. Oncogene 19, 5620–5635.

Brown MT, Cooper JA (1996). Regulation, substrates and functions of src. Biochim Biophys Acta 1287, 121–149.

Buss JE, Kamps MP, Gould K, Sefton BM (1986). The absence of myristic acid decreases membrane binding of p60src but does not affect tyrosine protein kinase activity. J Virol 58, 468–474.

Cao H, Courchesne WE, Mastick CC (2002). A phosphotyrosine-dependent protein interaction screen reveals a role for phosphorylation of caveolin-1 on tyrosine 14: recruitment of C-terminal Src kinase. J Biol Chem 277, 8771–8774.

Cary LA, Chang JF, Guan JL (1996). Stimulation of cell migration by overexpression of focal adhesion kinase and its association with Src and Fyn. J Cell Sci 109, 1787–1794.

Chetrit D, Ziv N, Ehrlich M (2009). Dab2 regulates clathrin assembly and cell spreading. Biochem J 418, 701–715.

Courtneidge SA (2002). Role of Src in signal transduction pathways. Biochem Soc Trans 30, 11–17.

del Pozo MA, Balasubramanian N, Alderson NB, Kiosses WB, Grande-Garcia A, Anderson RG, Schwartz MA (2005). Phospho-caveolin-1 mediates integrin-regulated membrane domain internalization. Nat Cell Biol 7, 901–908.

Donaldson JC, Dempsey PJ, Reddy S, Bouton AH, Coffey RJ, Hanks SK (2000). Crk-associated substrate p130(Cas) interacts with nephrocystin and both proteins localize to cell-cell contacts of polarized epithelial cells. Exp Cell Res 256, 168–178.

Efron B, Tibshirani R (1993). Estimates of bias. In: An Introduction to Bootstrap, ed. DR Cox, DV Hinkley, N Reid, DB Rubin, and BW Silverman, London: Chapman & Hall, 124–130.

Eisenberg S, Shvartsman DE, Ehrlich M, Henis YI (2006). Clustering of raft-associated proteins in the external membrane leaflet modulates internal leaflet H-Ras diffusion and signaling. Mol Cell Biol 26, 7190–7200.

Erpel T, Superti-Furga G, Courtneidge SA (1995). Mutational analysis of the Src SH3 domain: the same residues of the ligand binding surface are important for intra- and intermolecular interactions. EMBO J 14, 963–975.

Frame MC (2002). Src in cancer: deregulation and consequences for cell behaviour. Biochim Biophys Acta 1602, 114–130.

Frame MC (2004). Newest findings on the oldest oncogene; how activated src does it. J Cell Sci 117, 989–998.

Gaus K, Le Lay S, Balasubramanian N, Schwartz MA (2006). Integrin-mediated adhesion regulates membrane order. J Cell Biol 174, 725–734.

Glenney JR Jr, Soppet D (1992). Sequence and expression of caveolin, a protein component of caveolae plasma membrane domains phosphorylated on tyrosine in Rous sarcoma virus-transformed fibroblasts. Proc Natl Acad Sci USA 89, 10517–10521.

Glenney JR Jr, Zokas L (1989). Novel tyrosine kinase substrates from Rous sarcoma virus-transformed cells are present in the membrane skeleton. J Cell Biol 108, 2401–2408.

Grande-Garcia A, Echarri A, de Rooij J, Alderson NB, Waterman-Storer CM, Valdivielso JM, del Pozo MA (2007). Caveolin-1 regulates cell polarization and directional migration through Src kinase and Rho GTPases. J Cell Biol 177, 683–694.

Gutman O, Walliser C, Piechulek T, Gierschik P, Henis YI (2010). Differential regulation of phospholipase C-b_2 activity and membrane interaction by Ga_q, Gb_1g_2, and Rac2. J Biol Chem 285, 3095–3015.

Hancock JF (2006). Lipid rafts: contentious only from simplistic standpoints. Nat Rev Mol Cell Biol 7, 456–462.

Henis YI, Rotblat B, Kloog Y (2006). FRAP beam-size analysis to measure palmitoylation-dependent membrane association dynamics and microdomain partitioning of Ras proteins. Methods 40, 183–190.

Hill MM, Scherbakov N, Schiefermeier N, Baran J, Hancock JF, Huber LA, Parton RG, Parat MO (2007). Reassessing the role of phosphocaveolin-1 in cell adhesion and migration. Traffic 8, 1695–1705.

Ishizawar R, Parsons SJ (2004). c-Src and cooperating partners in human cancer. Cancer Cell 6, 209–214.

Jacobson K, Mouritsen OG, Anderson RG (2007). Lipid rafts: at a crossroad between cell biology and physics. Nat Cell Biol 9, 7–14.

Joshi B *et al*. (2008). Phosphorylated caveolin-1 regulates Rho/ROCK-dependent focal adhesion dynamics and tumor cell migration and invasion. Cancer Res 68, 8210–8220.

Kamps MP, Buss JE, Sefton BM (1985). Mutation of NH2-terminal glycine of p60src prevents both myristoylation and morphological transformation. Proc Natl Acad Sci USA 82, 4625–4628.

Kaplan KB, Swedlow JR, Varmus HE, Morgan DO (1992). Association of $p60^{c\text{-}Src}$ with endosomal membranes in mammalian fibroblasts. J Cell Biol 118, 321–333.

Kfir S, Ehrlich M, Goldshmid A, Liu X, Kloog Y, Henis YI (2005). Pathway- and expression level-dependent effects of oncogenic N-Ras: $p27^{Kip1}$ mislocalization by the Ral-GEF pathway and Erk-mediated interference with Smad signaling. Mol Cell Biol 25, 8239–8250.

Lee H *et al*. (2000). Constitutive and growth factor-regulated phosphorylation of caveolin-1 occurs at the same site (Tyr-14) in vivo: identification of a c-Src/Cav-1/Grb7 signaling cassette. Mol Endocrinol 14, 1750–1775.

Lee H, Woodman SE, Engelman JA, Volonte D, Galbiati F, Kaufman HL, Lublin DM, Lisanti MP (2001). Palmitoylation of caveolin-1 at a single site (Cys-156) controls its coupling to the c-Src tyrosine kinase: targeting of dually acylated molecules (GPI-linked, transmembrane, or cytoplasmic) to caveolae effectively uncouples c-Src and caveolin-1 (Tyr-14). J Biol Chem 276, 35150–35158.

Li S, Couet J, Lisanti MP (1996a). Src tyrosine kinases, Galpha subunits, and H-Ras share a common membrane-anchored scaffolding protein, caveolin. Caveolin binding negatively regulates the auto-activation of Src tyrosine kinases. J Biol Chem 271, 29182–29190.

Li S, Seitz R, Lisanti MP (1996b). Phosphorylation of caveolin by src tyrosine kinases: the a-isoform of caveolin is selectively phosphorylated by v-Src in vivo. J Biol Chem 271, 3863–3868.

Lin S, Naim HY, Rodriguez AC, Roth MG (1998). Mutations in the middle of the transmembrane domain reverse the polarity of transport of the influenza virus hemagglutinin in MDCK epithelial cells. J Cell Biol 142, 51–57.

Liu P, Rudick M, Anderson RG (2002). Multiple functions of caveolin-1. J Biol Chem 277, 41295–41298.

Machida K *et al*. (2007). High-throughput phosphotyrosine profiling using SH2 domains. Mol Cell 26, 899–915.

Martin GS (2001). The hunting of the Src. Nat Rev Mol Cell Biol 2, 467–475.

Melkonian KA, Ostermeyer AG, Chen JZ, Roth MG, Brown DA (1999). Role of lipid modifications in targeting proteins to detergent-resistant membrane rafts. Many raft proteins are acylated, while few are prenylated. J Biol Chem 274, 3910–3917.

Mitra SK, Schlaepfer DD (2006). Integrin-regulated FAK-Src signaling in normal and cancer cells. Curr Opin Cell Biol 18, 516–523.

Mukherjee A, Arnaud L, Cooper JA (2003). Lipid-dependent recruitment of neuronal Src to lipid rafts in the brain. J Biol Chem 278, 40806–40814.

Oneyama C, Hikita T, Enya K, Dobenecker MW, Saito K, Nada S, Tarakhovsky A, Okada M (2008). The lipid raft-anchored adaptor protein Cbp controls the oncogenic potential of c-Src. Mol Cell 30, 426–436.

Oneyama C, Iino T, Saito K, Suzuki K, Ogawa A, Okada M (2009). Transforming potential of Src family kinases is limited by the cholesterol-enriched membrane microdomain. Mol Cell Biol 29, 6462–6472.

Parat MO, Anand-Apte B, Fox PL (2003). Differential caveolin-1 polarization in endothelial cells during migration in two and three dimensions. Mol Biol Cell 14, 3156–3168.

Parton RG, Hanzal-Bayer M, Hancock JF (2006). Biogenesis of caveolae: a structural model for caveolin-induced domain formation. J Cell Sci 119, 787–796.

Place AT, Chen Z, Bakhshi FR, Liu G, O'Bryan JP, Minshall RD (2011). Cooperative role of caveolin-1 and C-terminal Src kinase binding protein

in C-terminal Src kinase-mediated negative regulation of c-Src. Mol Pharmacol 80, 665–672.
Radel C, Rizzo V (2005). Integrin mechanotransduction stimulates caveolin-1 phosphorylation and recruitment of Csk to mediate actin reorganization. Am J Physiol Heart Circ Physiol 288, H936–H945.
Razani B, Woodman SE, Lisanti MP (2002). Caveolae: from cell biology to animal physiology. Pharmacol Rev 54, 431–467.
Resh MD (1999). Fatty acylation of proteins: new insights into membrane targeting of myristoylated and palmitoylated proteins. Biochim Biophys Acta 1451, 1–16.
Resh MD (2006). Trafficking and signaling by fatty-acylated and prenylated proteins. Nat Chem Biol 2, 584–590.
Resh MD (2008). The ups and downs of SRC regulation: tumor suppression by Cbp. Cancer Cell 13, 469–471.
Robbins SM, Quintrell NA, Bishop JM (1995). Myristoylation and differential palmitoylation of the HCK protein-tyrosine kinases govern their attachment to membranes and association with caveolae. Mol Cell Biol 15, 3507–3515.
Rotblat B, Prior IA, Muncke C, Parton RG, Kloog Y, Henis YI, Hancock JF (2004). Three separable domains regulate GTP-dependent association of H-ras with the plasma membrane. Mol Cell Biol 24, 6799–6810.
Sambrook J, Russell DW (2001). Molecular Cloning: A Laboratory Manual, Cold Spring Harbor, NY: Cold Spring Harbor Laboratory Press.
Sandilands E, Brunton VG, Frame MC (2007). The membrane targeting and spatial activation of Src, Yes and Fyn is influenced by palmitoylation and distinct RhoB/RhoD endosome requirements. J Cell Sci 120, 2555–2564.
Sandilands E, Cans C, Fincham VJ, Brunton VG, Mellor H, Prendergast GC, Norman JC, Superti-Furga G, Frame MC (2004). RhoB and actin polymerization coordinate Src activation with endosome-mediated delivery to the membrane. Dev Cell 7, 855–869.
Schlaepfer DD, Hauck CR, Sieg DJ (1999). Signaling through focal adhesion kinase. Prog Biophys Mol Biol 71, 435–478.
Seed B, Aruffo A (1987). Molecular cloning of the CD2 antigen, the T-cell erythrocyte receptor, by a rapid immunoselection procedure. Proc Natl Acad Sci USA 84, 3365–3369.
Sharma DK, Brown JC, Choudhury A, Peterson TE, Holicky E, Marks DL, Simari R, Parton RG, Pagano RE (2004). Selective stimulation of caveolar endocytosis by glycosphingolipids and cholesterol. Mol Biol Cell 15, 3114–3122.
Shenoy-Scaria AM, Dietzen DJ, Kwong J, Link DC, Lublin DM (1994). Cysteine3 of Src family protein tyrosine kinase determines palmitoylation and localization in caveolae. J Cell Biol 126, 353–363.
Shvartsman DE, Donaldson JC, Diaz B, Gutman O, Martin GS, Henis YI (2007). Src kinase activity and SH2 domain regulate the dynamics of Src association with lipid and protein targets. J Cell Biol 178, 675–686.
Shvartsman DE, Gutman O, Tietz A, Henis YI (2006). Cyclodextrins but not compactin inhibit the lateral diffusion of membrane proteins independent of cholesterol. Traffic 7, 917–926.
Shvartsman DE, Kotler M, Tall RD, Roth MG, Henis YI (2003). Differently-anchored influenza hemagglutinin mutants display distinct interaction dynamics with mutual rafts. J Cell Biol 163, 879–888.
Simons K, Toomre D (2000). Lipid rafts and signal transduction. Nat Rev Mol Cell Biol 1, 31–39.
Tansey MG, Baloh RH, Milbrandt J, Johnson EM Jr (2000). GFRa-mediated localization of RET to lipid rafts is required for effective downstream signaling, differentiation, and neuronal survival. Neuron 25, 611–623.
Urra H, Torres VA, Ortiz RJ, Lobos L, Diaz MI, Diaz N, Hartel S, Leyton L, Quest AF (2012). Caveolin-1-enhanced motility and focal adhesion turnover require tyrosine-14 but not accumulation to the rear in metastatic cancer cells. PLoS One 7, e33085.
Veracini L, Franco M, Boureux A, Simon V, Roche S, Benistant C (2006). Two distinct pools of Src family tyrosine kinases regulate PDGF-induced DNA synthesis and actin dorsal ruffles. J Cell Sci 119, 2921–2934.
Volonte D, Galbiati F, Pestell RG, Lisanti MP (2001). Cellular stress induces the tyrosine phosphorylation of caveolin-1 (Tyr^{14}) via activation of p38 mitogen-activated protein kinase and c-Src kinase. Evidence for caveolae, the actin cytoskeleton, and focal adhesions as mechanical sensors of osmotic stress. J Biol Chem 276, 8094–8103.
Wary KK, Mariotti A, Zurzolo C, Giancotti FG (1998). A requirement for caveolin-1 and associated kinase Fyn in integrin signaling and anchorage-dependent cell growth. Cell 94, 625–634.
Webb DJ, Donais K, Whitmore LA, Thomas SM, Turner CE, Parsons JT, Horwitz AF (2004). FAK-Src signalling through paxillin, ERK and MLCK regulates adhesion disassembly. Nat Cell Biol 6, 154–161.
Wolfenson H, Lubelski A, Regev T, Klafter J, Henis YI, Geiger B (2009). A role for the juxtamembrane cytoplasm in the molecular dynamics of focal adhesions. PLoS One 4, e4304.
Yeo MG, Partridge MA, Ezratty EJ, Shen Q, Gundersen GG, Marcantonio EE (2006). Src SH2 arginine 175 is required for cell motility: specific focal adhesion kinase targeting and focal adhesion assembly function. Mol Cell Biol 26, 4399–4409.